Transonic Solutions for a Multielement Airfoil Using the Full-Potential Equations

J. Flores,* T. L. Holst,* and R. L. Sorenson*
NASA Ames Research Center, Moffett Field, California

Transonic flow solutions are obtained over a multielement airfoil (augmentor-wing) using the full-potential equation. Solutions obtained for a subcritical case and a strong-shock case show good quantitative agreement with experiment in regions not dominated by viscous effects. In those regions where viscous effects are dominant, the results are still in good qualitative agreement. For the strong-shock case, Mach-number and angle-of-attack corrections were necessary to match experimental C_L. Typical results from the transonic augmentor-wing potential code (TAUG) on the Cray-1S computer require about 10 s of CPU time for a three-order-of-magnitude drop in the maximum residual. The speed with which solutions can be generated and the associated low cost will make this code a practical tool for the design aerodynamicist.

Introduction

SINCE its conception by de Havilland Aircraft of Canada,[1] the 18%-thick augmentor-wing (see Fig. 1) has been described as having several advantages over more conventional, single-foil supercritical sections of the same overall thickness-to-cord ratio. Some of these potential advantages are higher drag-rise Mach number, lower-form drag of the main-airfoil section, and increased buffet boundaries.[2] The augmentor-wing configuration has also been viewed as a new type of powered-lift approach with significant benefits resulting from the integration of powerplant and wing designs.[3] It has also been observed experimentally that the augmentor-wing in cruise configuration with blowing can contribute major savings in aircraft fuel consumption through its increased aerodynamic efficiency.

Simulation of a flowfield by means of wind-tunnel experiments and computers are the two basic tools in configuration design. Although wind-tunnel experiments can be used to investigate complex configurations and aerodynamic phenomena, problems such as wall and support interference, model distortion, operating-range limitations, and flow nonuniformity can lead to inadequate simulation. Thus, some military aircraft problems discovered only in flight test (incorrectly predicted wing flow, drag-rise Mach number, transonic airframe drag, etc.) affect aircraft cost and result in delayed or reduced operational capabilities.[4] Some of these problems could be avoided by using today's computational capability.

Ways in which computations can complement experiment include test facility error corrections, data for conditions beyond experimental operating range, flow physics, and configuration optimization. A 20% improvement in fuel efficiency of the Airbus A-310 over that of the A-300 is attributed primarily to the use of computational aerodynamics.[4] Thus, computer codes are rapidly becoming instrumental not only in increasing understanding of flow physics and near-optimal design configurations but, perhaps more importantly, in reducing costs relative to the rising costs of wind-tunnel experiments. It is with this thought in mind that the present work was embarked upon.

TAUG was developed to investigate the improved efficiencies of the augmentor-wing at the cruise configuration. Although experimental and numerical results[5] indicate some separation in the channel regions between the main airfoil and the shrouds, there is a potentially large demand for an inviscid code to analyze augmentor-wing geometries. It is anticipated that in most good augmentor-wing designs viscous effects will be minimal. In addition, the pressure gradients resulting from an inviscid computation can be used (qualitatively) to estimate regions of separation and thus help to determine what constitutes a good or bad design. Therefore, because typical run times associated with the inviscid full-potential formulation may be orders of magnitude less expensive than other viscous procedures, many different geometrical or flow parameters can be investigated. TAUG, for example, can generate solutions (default case $M_\infty = 0.7$, $\alpha = 1.05$ deg) in approximately 10 s, whereas 2 h may be required for a Navier-Stokes solution[5] on a Cray-1S computer. Thus, an inviscid code, such as TAUG, would allow the design aerodynamicist to focus in on a near-optimal augmentor-wing configuration with inexpensive computational solutions.

Earlier works on multielement airfoils for transonic flowfields were limited to airfoils with a maximum number of two elements.[6-9] The governing equations used were the small-disturbance equations,[6] the Navier-Stokes equations,[7] or the nonconservative full-potential equation.[8,9] Later efforts[10,11] eliminated the restriction of a maximum of two elements and solved the flow over a three-element airfoil. The governing equations used were also the nonconservative full-potential equation. The arrangement of the three-element airfoils comprised a main airfoil with one of the following: 1) a trailing lower flap, 2) a leading-edge slat, or 3) a combination of the two.

The multielement airfoil for this study, however, has a completely different geometric topology (see Fig. 1). It consists of a main airfoil (and a slot opening at the trailing edge for jet blowing) with two smaller aft airfoils, or shrouds. The shrouds are positioned to form a channel-like region and thus act as an ejector (or thrust augmenter) for the blowing case. (In the present study only cases without blowing will be considered.)

Presented as Paper 84-0300 at the AIAA 22nd Aerospace Sciences Conference, Reno, Nev., Jan. 9-12, 1984; received Feb. 18, 1984; revision received June 26, 1984. This paper is declared a work of the U.S. Government and therefore is in the public domain.

*Research Scientist. Member AIAA.

Theoretical Background

In the present study, transonic-flow solutions over the augmentor-wing are obtained by solving the full-potential equation. The TAIR (Transonic AIRfoil analysis) full-potential code[12] was modified to solve the multielement airfoil configurations of the augmenter-wing type. This code uses a fully implicit approximate-factorization (AF2) scheme to solve the transformed full-potential equation in a general, nonorthogonal, body-conforming coordinate system. The full-potential equation written in strong conservation-law form is given by

$$(\rho\phi_x)_x + (\rho\phi_y)_y = 0 \tag{1a}$$

$$\rho = \left[1 - \frac{\gamma-1}{\gamma+1}(\phi_x^2 + \phi_y^2)\right]^{1/\gamma-1} \tag{1b}$$

where the velocity components (ϕ_x and ϕ_y) and the density ρ are nondimensionalized by the critical sound speed α_* and the stagnation density ρ_s, respectively; x and y are the Cartesian coordinates; and γ is the ratio of specific heats.

Mass conservation is expressed by Eq. (1) for flows that are isentropic and irrotational. For many transonic-flow applications, the corresponding shock-jump conditions are valid approximations to the Rankine-Hugoniot relations.[13]

To transform Eq. (1) from the physical domain (Cartesian coordinates) into a computational domain, a general nonorthogonal, independent-variable transformation is used. This general transformation,

$$\xi = \xi(x,y) \qquad \eta = \eta(x,y) \tag{2}$$

maintains the strong conservation-law form of Eq. (1). The full-potential equation written in the computational domain (ξ, η coordinate system) is given by

$$(\rho U/J)_\xi + (\rho V/J)_\eta = 0 \tag{3a}$$

$$\rho = \left[1 - \frac{\gamma-1}{\gamma+1}(A_1\phi_\xi^2 + 2A_2\phi_\xi\phi_\eta + A_3\phi_\eta^2)\right]^{1/\gamma-1} \tag{3b}$$

where

$$U = A_1\phi_\xi + A_2\phi_\eta$$

$$V = A_2\phi_\xi + A_3\phi_\eta \tag{4}$$

and

$$A_1 = \xi_x^2 + \xi_y^2 = \nabla\xi\nabla\xi$$

$$A_2 = \xi_x\eta_x + \xi_y\eta_y = \nabla\xi\nabla\Delta\eta$$

$$A_3 = \eta_x^2 + \eta_y^2 = \nabla\eta\nabla\eta \tag{5}$$

$$J = \xi_x\eta_y - \xi_y\eta_x = 1/(x_\xi y_\eta - x_\eta y_\xi) \tag{6}$$

The U and V terms are the contravariant components along the ξ and η directions, respectively; A_1, A_2, and A_3 are metric quantities; and J is the Jacobian of the transformation. The following metric identities are necessary in numerically evaluating the above expressions:

$$\xi_x = Jy_\eta \qquad \eta_x = -Jy_\xi$$

$$\xi_y = -Jx_\eta \qquad \eta_y = Jx_\xi \tag{7}$$

Grid Description and Code Modifications

Grid Description

The grid for the augmentor-wing configuration is generated utilizing GRAPE (GRids about Airfoils using Poisson's Equations) program.[14,15] An example grid, which consists of 106×35 points in the wrap-around (ξ) and normal-like (η) directions, respectively, is shown in Fig. 1. The grid topology about the main airfoil is of the C-type; that about each of the shrouds is of the H-type. The GRAPE program generates this grid in two separate sections. The first grid section consists of the innermost ξ-grid lines between the main airfoil and the shrouds (a total of seven ξ-grid lines for the grid of Fig. 1). The second grid section consists of all ξ-grid lines between the shrouds and the outer boundary. Control of the spacing and orthogonality at all boundaries is accomplished by the iterative solution of two coupled Poisson differential equations. For a more detailed description of the grid-generating procedure, the reader is referred to Ref. 5.

The ξ computational variable increases in a clockwise manner, and the η variable increases from the outer boundary to the inner boundary. The ξ-direction corresponds to the i index and varies from 1 to $imax$. The η direction corresponds to the j index and varies from 1 to $jmax$. Each grid-point position is thus identified with an (i,j) index pair. The outer grid boundary has three parts, $\partial\Omega_1$, $\partial\Omega_2$, and $\partial\Omega_3$. Those points lying in the set $i=1$, $2\le j\le jmax$ belong to the boundary $\partial\Omega_1$. The boundary $\partial\Omega_2$ contains those points $j=1$, $1\le i\le imax$. Finally, $\partial\Omega_3$ are those points such that $i=imax$ and $2\le j\le jmax$. The boundary $\partial\Omega_2$ is the outer freestream

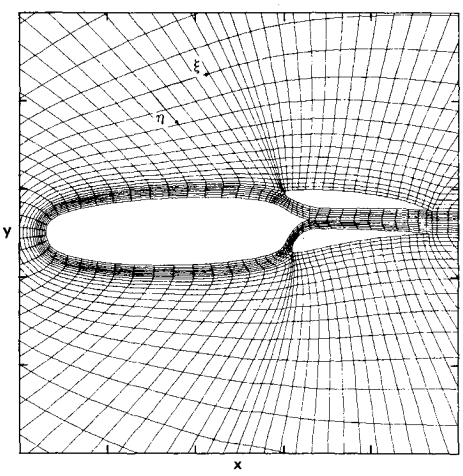

Fig. 1 Augmentor-wing finite difference grid.

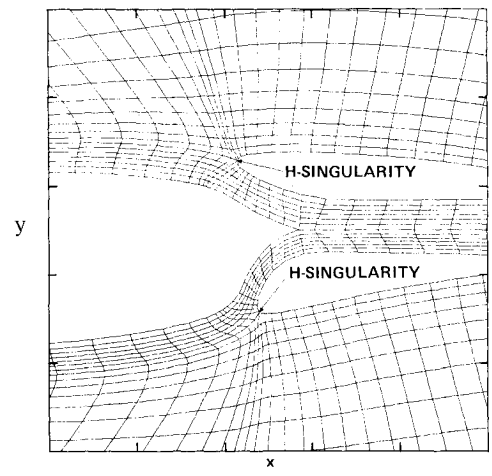

Fig. 2 Expanded view of jet area.

boundary, and the boundaries $\partial\Omega_1$ and $\partial\Omega_3$ are the lower and upper outflow boundaries, respectively.

The airfoil surface boundary condition is that of flow tangency (i.e., no flow through the airfoil surface), which requires that the η contravariant velocity component at the airfoil surface be zero (i.e., $V=0$). This boundary condition is implemented by aplying

$$(\rho V/J)_{ibod,jbod-1/2} = -(\rho V/J)_{ibod,jbod+1/2} \tag{8}$$

where $i=ibod$, $j=jbod$ denotes a grid point on one of the three airfoil surfaces. In those expressions in which ϕ_η is required at the airfoil surface, the $V=0$ boundary condition is used again to obtain

$$\phi_\eta|_{\text{surface}} = -A_2/A_3\phi_\xi|_{\text{surface}} \tag{9}$$

In addition, ϕ must be allowed a discontinuity equal to Γ in crossing the double-stored ξ line downstream of the trailing edge of each airfoil surface. The magnitude of Γ (different for each airfoil surface) is determined by the Kutta condition, which requires that the upper and lower surface pressures be equal at the trailing edge of the airfoils.

Inherent in the local grid about the leading edge of each shroud is an H-type singularity (see Fig. 2). This singularity causes large amounts of skewness and stretching but should cause little difficulty since the geometric error introduced into the true solution can be minimized by appropriately differencing the metric quantities associated with the transformation.[16] Reference 16 illustrates, in detail, how the local accuracy around grid singularities and global error associated with, for example, the lift are improved. A comparative study of solutions (generated on grids which were smooth to grids which were nonsmooth, highly stretched, and/or skewed) led to the conclusions of Ref. 16.

Code Modifications

The TAIR code uses an approximate-factorization (AF2) scheme and is given by Step 1:

$$(\alpha+\vec{\delta}_\eta B_j)f^n_{i,j} = -\alpha\omega L\phi^n_{i,j} \tag{10a}$$

Step 2:

$$(\alpha\overleftarrow{\delta}_\eta \mp \alpha\beta\vec{\delta}_\xi + \overleftarrow{\delta}_\xi B_i\vec{\delta}_\xi)C^n_{i,j} = f^n_{i,j} \tag{10b}$$

where

$$B_i = \left(\frac{\rho^n A_1}{J}\right)_{i+1/2,j} \qquad B_j = \left(\frac{\rho^n A_3}{J}\right)_{i,j-1/2} \tag{11}$$

and one-sided difference operators for the ξ direction are defined by

$$\vec{\delta}_\xi(\ )_{i,j} = (\ )_{i+1,j} - (\ )_{i,j} \qquad \text{forward}$$

$$\overleftarrow{\delta}_\xi(\ )_{i,j} = (\ )_{i,j} - (\ )_{i-1,j} \qquad \text{backward}$$

The η-difference operators can be obtained by symmetry. The ω term is a relaxation parameter, and α is an acceleration parameter (that can be regarded as Δt^{-1}). A small value of α (i.e., too large a time-step) can result in divergence of the iteration scheme. For a more detailed description of the AF2 algorithm, the reader is referred to Ref. 12.

Three major modifications were required to transform the base code TAIR into the multielement airfoil code TAUG. The first involved changing the O-grid topology to a C-type topology with additional logic to enforce the proper flow-tangency boundary conditions at the upper and lower shroud surfaces. This required modifying the boundary conditions of Eqs. (10a) and (10b) to be compatible with a C-type topology. Thus, in Step 1 [Eq. (10a)], the main airfoil wake was included along the $j=jmax$ boundary. Previously, in the O-grid topology, the $j=jmax$ boundary consisted of only the airfoil suface. In Step 2 [Eq. (10b)], the endpoints of the tridiagonal inversion were changed to lie along $\partial\Omega_1$ and $\partial\Omega_3$. In the O-mesh version the endpoints for the Step 2 tridiagonal matrix were periodic.

The shroud logic complicates the conversion process in several ways. First, all the bidiagonal inversions in the η direction (Step 1) have to account appropriately for the double-stored ξ line which contains the shroud surfaces. That is, two separate inversions are implemented in the η direction when a shroud is encountered (see Fig. 2 for examples of η-grid lines that intersect the shroud surfaces). Second, the ξ-matrix inversion along this double-stored ξ line must be inverted twice: once along the entire ξ line, including the lower surface of the lower shroud and the upper surface of the upper shroud; and once separately for only the upper surface of the lower shroud and the lower surface of the upper shroud. With this modification, every grid point in the multielement airfoil grid is updated in an implicit manner.

The second major modification was implemented to enhance stability of the AF2 interation scheme for a C-type topology. At the main airfoil (and along the main airfoil wake) $\vec{\delta}_\eta f^n = 0$ is used as an intermediate boundary condition for Step 1. This boundary condition is required at the $j=jmax$ boundary because values of f at $i,jmax+1$ are unknown and difficult to obtain. Lack of a good physical interpretation of f makes the formation of a more logical boundary condition difficult. The only criterion that f must satisfy is that as the iteration process drives the solution to a steady state, f must approach zero.

A stability analysis[17] shows that for the $\vec{\delta}_\eta f^n = 0$ condition, a severe restriction is placed on α at the airfoil surface, namely

$$\alpha > A_3\omega \tag{12}$$

For the O-mesh version of TAIR, this restriction posed no real problems since the A_3 metric was of the order 1. Special logic in the TAIR computer code empirically forced α at the $j=jmax$ boundary to always satisfy Eq. (12). But for the C-mesh version, the A_3 metric was orders of magnitude larger, thus requiring large values of α and small values of the effective time-step. This tended to slow convergence drastically.

Reference 17 suggested another way of imposing the intermediate boundary condition for f such that $\vec{\delta}_\eta f^n \neq 0$. Let a "dummy point" value for f be given as

$$f^n_{i,jmax+1} = \theta\, f^n_{i,jmax} \qquad 1 \le i \le imax \tag{13}$$

where $jmax$ denotes the airfoil surface (or the airfoil/wake surface for the C-mesh topology) and $jmax+1$ denotes a fictitious point inside the airfoil surface. Choosing $\theta=-1$, a stability analysis reveals unconditional stability for the AF2 scheme; that is,

$$\alpha \ge 0 \qquad 0 \le \omega \le 2.0 \tag{14}$$

This modification allows larger time-steps and improves convergence (especially for the C-mesh version) of the AF2 iteration scheme.

The last modification consisted of changing the outer boundary condition (see Ref. 12 for a complete discussion of the old boundary condition). The new boundary condition consists of imposing $\phi=\phi_\infty$ on the boundary $\partial\Omega_2$. On the upper outflow boundary ($\partial\Omega_3$), $\phi^{n+1}_{i,j}$ is extrapolated to determine $\phi^{n+1}_{imax,j}$ ($2\le j\le jmax$). The extrapolation formula is determined by the condition

$$\phi^{n+1}_x|_{imax-\frac{1}{2},j}=\phi^{n+1}_x|_{imax-3/2,j} \qquad 2\le j\le jmax \quad (15a)$$

This equation, differenced in general coordinates, becomes

$$\xi_x|_{imax-\frac{1}{2},j}(\phi^{n+1}_{imax,j}-\phi^{n+1}_{imax-1,j})=\xi_x|_{imax-3/2,j}(\phi^{n+1}_{imax-1,j}-\phi^{n+1}_{imax-2,j})$$
$$2\le j\le jmax \quad (15b)$$

and is implemented implicitly in the tridiagonal inversion required by Eq. (10b). Utilizing Eq. (15b) and the fact that $C^n_{i,j}=\phi^{n+1}_{i,j}-\phi^n_{i,j}$ yields

$$(C^n_{imax,j}-C^n_{imax-1,j})=\text{Ratio}_j\,(C^n_{imax-1,j}-C^n_{imax-2,j})$$
$$2\le j\le jmax \quad (16)$$

where

$$\text{Ratio}_j=\left(\frac{\xi_x|_{imax-3/2,j}}{\xi_x|_{imax-\frac{1}{2},j}}\right)$$

To eliminate $C^n_{imax,j}$, Eq. (16) is evaluated at $i=imax-1$ and combined with the tridiagonal equation given by Eq. (10b):

$$B\cdot C^n_{imax-2,j}+D\cdot C^n_{imax-1,j}+A\cdot C^n_{imax,j}=f^n_{imax-1,j} \quad (17)$$

This yields

$$(B-A\cdot\text{Ratio}_j)\cdot C^n_{imax-2,j}+[D+A\cdot(\text{Ratio}_j+1)]\times C^n_{imax-1,j}=f^n_{imax-1,j} \quad (18)$$

where A, D, and B are the tridiagonal elements obtained from Eq. (10b). This equation, with two values in the unknown correction vector ($C^n_{imax-2,j}$ and $C^n_{imax-1,j}$), becomes the final equation in the ξ-direction tridiagonal matrix equation. A similar procedure is implemented for the $\partial\Omega_1$ boundary where the $C^n_{1,j}$ term is eliminated. The outer boundary condition modification just presented is primarily required because of the new C-mesh grid topology, but also served to speed convergence by setting up the lift at a faster rate. The motivation for the new outer boundary condition was as follows. At the outflow boundaries, far enough downstream, we expect $u=u_\infty$ and $v=0$ from physical intuition. This is reflected numerically from the extrapolation procedure, which is $\partial/\partial\xi(\phi_x)=0$

Discussion of Results

In Fig. 3 computational results are compared with experiment[18] for a flow with a freestream Mach number of 0.7 and an angle of attack of 1.05 deg. Upward- and downward-facing triangles denote experimental data for the upper and lower surfaces, respectively. The pressure-coefficient distributions for the upper and lower shrouds have been displaced by +1 and −1, respectively. There is also a shift to the right in x/c for the data of the shrouds. The lower surface C_P distribution and the crossover of the upper and lower pressure distributions are both nicely captured on the main airfoil. The upper-surface pressure distribution, although qualitatively correct, is in slight disagreement with experiment. In the thin-layer Navier-Stokes solution of Ref. 5, this disagreement is greater and was attributed to the need of an angle-of-attack correction in the experiment.

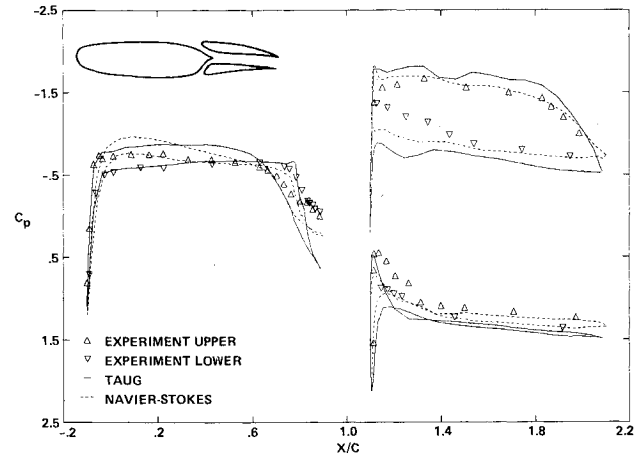

Fig. 3 C_P distribution on airfoils; $M_\infty=0.7$, $\alpha=1.05$ deg.

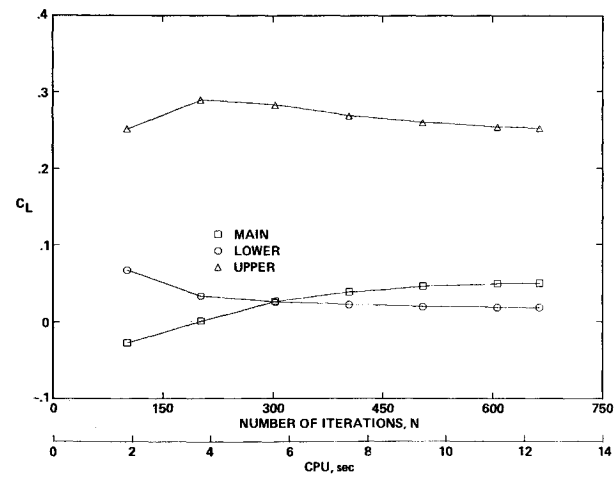

Fig. 4 C_L history vs number of iterations; $M_\infty=0.7$, $\alpha=1.05$ deg.

The results for the upper shroud are qualitatively in good agreement with experimental data. The discrepancy in the lower part of the leading edge, which is also partially reproduced in the Navier-Stokes results of Ref. 5, can probably be attributed to viscous effects in the channel between the main airfoil and the upper shroud. That is, either the lack of viscous effects (full-potential) or the lack of an adequate turbulence model (Navier-Stokes) is causing the discrepancy with experiment. The bumps in the upper-surface pressure distribution exist in both the present full-potential and the Navier-Stokes results of Ref. 5 and thus lead to the speculation that the body coordinates of the upper shroud may not be smooth.

The peak C_P at the leading edge of the lower shroud is successfully captured; however, poor quantitative results occur on the upper-surface distribution. This may again be the result of viscous effects which occur in the lower channel region between the main airfoil and the lower shroud. The Navier-Stokes solution of Ref. 5 did predict small regions of separated flow in both channel regions with a slightly stronger separation in the lower channel.

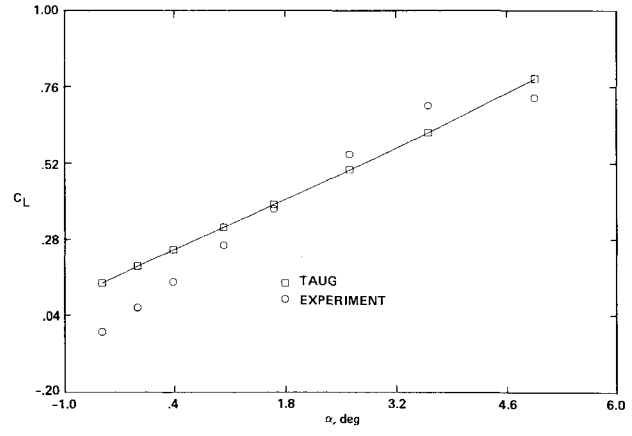

Fig. 5 C_L vs α; $M_\infty = 0.7$.

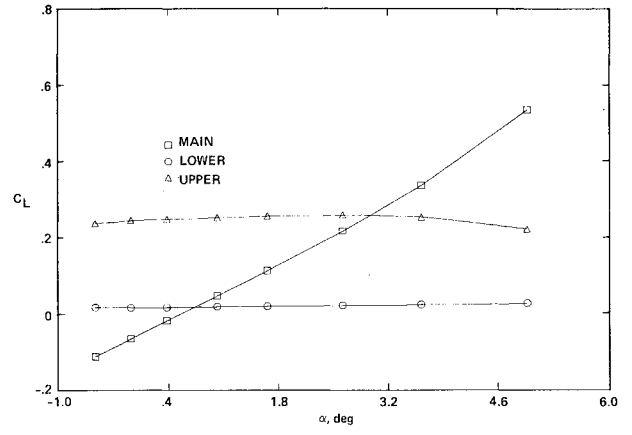

Fig. 6 Individual C_L vs α; $M_\infty = 0.7$.

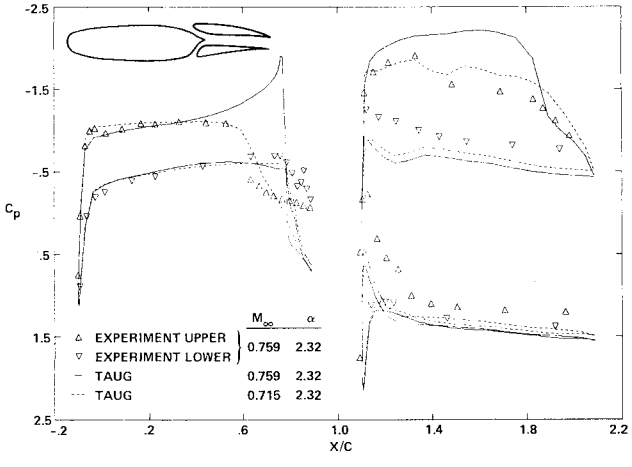

Fig. 7 C_P **distribution on airfoils.**

As mentioned earlier, the pressure gradients resulting from the inviscid solution can lend insight into regions of possible separation. At the trailing edge of the main airfoil, high pressure gradients can be seen. The pressure gradient is greater on the lower surface than on the upper surface. This would indicate a larger separation region on the lower surface (at the trailing edge) than on the upper surface. This is in fact verified with the "separation" contours of Ref. 5. Note also the high pressure gradient on the upper shroud (upper surface at the trailing edge) indicating a region of separation which again was verified numerically.[5]

Figure 4 displays lift vs iteration number and CPU time (Cray-1S computer) for each of the three individual lifting surfaces. The lift associated with each surface approaches an asymptotic limit after about 600 iterations. This number of iterations is about an order of magnitude larger than usually required by the base TAIR code for single-airfoil applications. This difference is probably a result of additional "stiffness" generated by the augmentor-wing channel regions. Nevertheless, it is anticipated that a significant reduction in the number of iterations required for convergence by the TAUG code can be obtained with additional research.

The main airfoil lift in Fig. 4 starts with a negative value and eventually approaches a small positive asymptotic limit. The lower shroud lift starts small and decreases, eventually crossing the main airfoil value of lift. The upper shroud contributes the largest component of lift to the augmentor-wing and attains this value quickly. Despite the fact that the Navier-Stokes code of Ref. 5 utilized a time-accurate algorithm whereas the present algorithm is not time-accurate, these general lift convergence characteristics are the same for both approaches.

The solution convergence history displayed in Fig. 4 indicates adequate convergence after about 10 s of computer time (106 × 35 mesh). To evaluate this time fully, it should be noted that the TAUG code has been partially vectorized on the Cray-1S computer. The OFF = V/ON = V ratio, which is a measure of how well a code is vectorized, is about 3.0 for the TAUG code (that is, the speed of the code without benefit of vector instructions is 3.0 times slower than the speed with vector instructions). Since a fully vectorized code might produce an OFF = V/ON = V ratio as high as 5.0, it can be seen that the level of vector efficiency is about 60%. With this level of efficiency, the TAUG code is about 6 times faster on the Cray-1S computer than on the CDC 7600 machine. The present approach is about 1,000 times faster than the Navier-Stokes approach of Ref. 5. However, the present approach is inviscid and does not include viscous effects, as does the Navier-Stokes solution of Ref. 5. The speed with which the present potential method can generate solutions and the associated low cost will allow the TAUG code to be a practical tool to the design aerodynamicist.

Figure 5 shows a comparison of the lift vs angle of attack for the augmentor-wing configuration at a freestream Mach number of 0.7. The lift curve slope agreement is only fair. However, a reevaluation of the experimental angle-of-attack correction indicated a shift in the experimental slope which would bring the two results into better agreement.[19] The stall angle for the experimental data appears to be about 4 deg. Of course, this viscous phenomenon does not occur for the inviscid solution.

Another physically interesting aspect of the augmentor-wing (observed experimentally) is the apparent insensitivity of shroud lift to angle of attack. Figure 6 shows that TAUG is successful in capturing this physical characteristic. It can be observed that the lift of each shroud varies only slightly with angle of attack; however the main-airfoil lift increases linearly.

A strong-shock case with a Mach number of 0.759 and an angle of attack of 2.32 deg is shown in Fig. 7. The solid lines indicate results obtained at the experimental values of Mach number and angle of attack. The upward- and downward-facing triangles retain the same definition as before (upper and lower surfaces, respectively). As can be seen, the results are in poor agreement with experiment. On the main airfoil, the shock position deviates from experiment by about 20% chord. The magnitude of the shock strength is greater than the experimental value by a factor of about two. Similarly, the upper and lower shroud pressure distributions are off by significant amounts.

The dashed lines shown in Fig. 7 indicate numerical results obtained at $M_\infty = 0.715$ and $\alpha = 2.32$ deg. As can be seen,

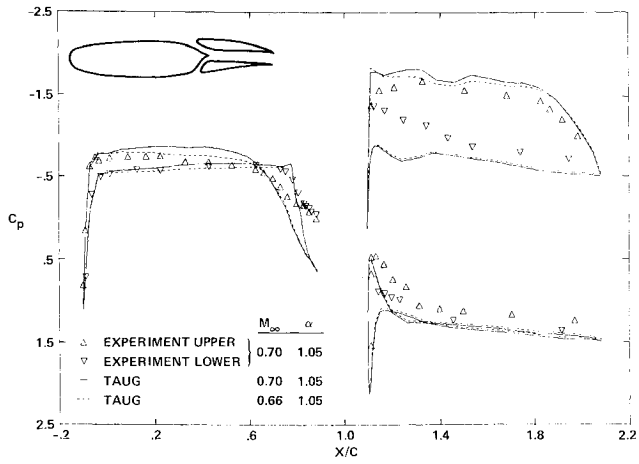

Fig. 8 C_P distribution on airfoils.

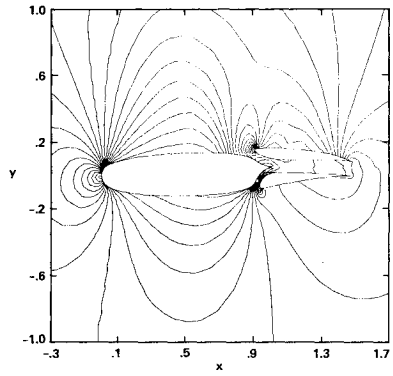

Fig. 9 Density contours; $M_\infty = 0.715$, $\alpha = 2.32$ deg.

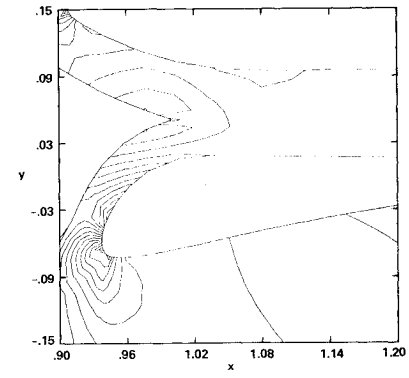

Fig. 10 Density contours of expanded jet area; $M_\infty = 0.715$, $\alpha = 2.32$ deg.

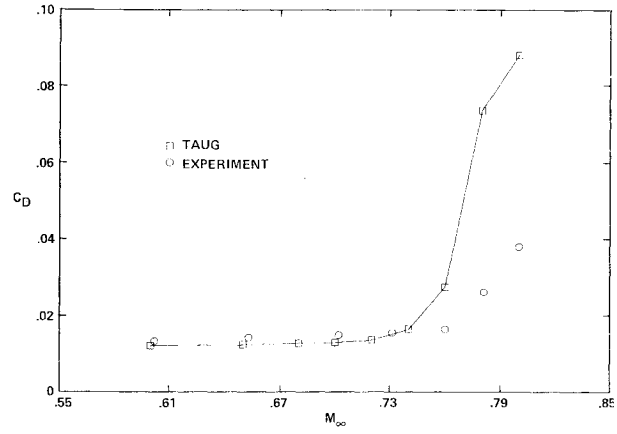

Fig. 11 Drag-rise Mach curve; $\alpha = 1.05$ deg.

correcting the Mach number in this way yielded excellent agreement between the numerical and experimental results (at least in regions of the solution not dominated by viscous effects). On the main airfoil, the leading-edge peak pressure is captured as is the position of the shock. The lower-surface pressure distribution and the crossover characteristic are also successfully captured.

On the shrouds the corrected numerical and experimental pressure distributions are in good qualitative agreement. The best agreement exists on the upper surface of the upper shroud and on the lower surface of the lower shroud. Between the shrouds, where viscous effects are probably significant, the agreement is only fair. Note how the Mach-number correction improves the solution at almost every location on all three airfoil elements.

In other cases, the need for a large Mach-number correction appeared to be the trend. The corrected Mach number was consistently lower than the given experimental Mach number. In the stronger-shock cases, large changes in the solution resulted from the Mach-number correction. For the weak-shock or subcritical cases, the Mach-number correction was not as important but did generally produce better agreement with experiment. For example, the slightly supercritical case shown in Fig. 3, which did not require a Mach-number correction to produce reasonable agreement with experiment, did show an improvement in accuracy with a -0.04 correction in the freestream Mach number. The uncorrected (solid lines) and corrected (dashed lines) solutions are compared with experimental results in Fig. 8. Note that the dashed solution is better than the solid solution at almost every location. Of course, the dashed solution is still not good in the channel regions where viscous effects are important.

Undoubtedly, some of this Mach-number correction is required to eliminate numerical errors. For example, the numerical error generated by not modeling viscous effects can be simplistically eliminated by angle-of-attack or Mach-number corrections or both (at least for standard airfoil calculations). Another source of error is due to the lack of modeling entropy effects, inherent in the full-potential formulation, which would tend to produce stronger shocks. A study which will attempt to quantify the effect of both of these sources of error is currently in progress. The last likely source of error requiring Mach-number and angle-of-attck corrections is from the experiment, for example, wind-tunnel-wall interference. It is not likely, however, that the Mach-number correction for this experiment is more than -0.0005.[19]

Figure 9 shows density contours for the augmentor-wing for the $M_\infty = 0.715$ and $\alpha = 2.32$ deg case. The stagnation areas and the upper-surface shock are easily identified. Figure 10 shows an expanded view of the throat area. The rapid expansion at the leading edge of the lower shroud and the large compression gradient at the inlet of the lower shroud are clearly visible. Large separation, as mentioned previously, was observed numerically in this region for the Navier-Stokes simulation of Ref. 5.

The smearing of the main-airfoil shock in Fig. 9 is caused primarily by the coarseness of the mesh. On the main airfoil there are a total of 60 points, while the shrouds have a total of 40 points each. This effectively puts about 30 points on the upper surface of the main airfoil. More points would be required to produce a "sharper" shock.

Figure 11 shows a comparison of the coefficient of drag vs freestream Mach number. The angle of attack was fixed at 1.05 deg for all cases presented. The numerical results plot

only pressure drag, whereas the experimental results are for total drag. Emphasis should not be placed on the lower end of the Mach-number spectrum because, for these subcritical cases, potential theory should predict zero drag. Therefore, the plotted potential drag for the lower Mach-number cases is really an indication of the numerical error associated with the algorithm or the finite-difference grid (primarily grid coarseness and distortion). If the 0.04 Mach-number correction determined from Fig. 7 is applied to Fig. 11, then the numerical and experimental values for the drag-divergence Mach number are almost identical.

Conclusions

A full-potential code for solving transonic flow over a multielement airfoil has been developed and successfully applied to compute the transonic flow over the augmentor-wing. Surface-pressure-coefficient comparisons for several cases show good quantitative agreement with experiment in regions not dominated by viscous effects, providing the proper Mach-number corrections are implemented. Other results, including total C_L vs α, C_L vs α for each individual airfoil element, and drag-divergence Mach number, all show good qualitative agreement with experiment.

The potential code has been implemented on the Cray-1S vector computer and can generate solutions in about 10 s (on a grid size of 106×35). The speed at which solutions can be generated allows a variety of flow parameters and geometrical designs to be quickly analyzed. Near optimal augmentor-wing configurations can be determined in an efficient and inexpensive manner, making the code an amenable tool for the design aerodynamicist.

References

[1] "Analysis of Results from Test of an Asymmetric High Speed Augmentor-Wing Model (WTCB) in the NAE Two-Dimensional High Reynolds Number Blowdown Tunnel," DHC-DIR 75-2, de Havilland Aircraft of Canada, Limited, Aug. 1975.

[2] Farbridge, J. E. and Smith, R. C., "The Transonic Multi-Foil Augmentor-Wing," AIAA Paper 77-606, Palo Alto, Calif., 1977.

[3] Whittley, D. C., "Augmentor-Wing Technology for STOL Transport Aircraft," presented for the High Lift Technology course at the University of Tennessee Space Institute, Tullahoma, Tenn., Oct. 27-31, 1975.

[4] Ballhaus, W. F., "Supercomputing in Aerodynamics," presented at the Conference on Frontiers of Supercomputing, Los Alamos, N. Mex., Aug. 15-19, 1983.

[5] Lasinski, T. A., Andrews, A. E. et al., "Computation of the Steady Viscous Flow over a Tri-Element 'Augmentor-Wing' Airfoil," AIAA Paper 82-0021, Orlando, Fla., 1982.

[6] Caughey, D. A., "An Inviscid Analysis of Transonic Slatted Airfoils," AIAA Paper 74-541, 1974.

[7] Thames, F. C., Thompson, J. F., and Mastin, C. W., "Numerical Solution of the Navier-Stokes Equation for Arbitrary Two-Dimensional Airfoils," Aerodynamic Analysis Requiring Advanced Computers, Part I, NASA SP-347, 1975.

[8] Grossman, B. and Melnik, R. E., "The Numerical Computation of the Transonic Flow over Two-element Airfoil Systems," 5th International Conference on Numerical Methods in Fluid Dynamics, Enschede, The Netherlands, June 28-July 3, 1976.

[9] Arlinger, B. C., "Analysis of Two-element High Lift Systems in Transonic Flow," ICAS Paper No. 76-13, Oct. 1976.

[10] Klevenhusen, K. D., "A Calculation Method for Multielement Airfoils in Subsonic and Transonic Potential Flow," AIAA Paper 80-0340, 1980.

[11] Rosch, H. and Klevenhusen, K. D., "Flow Computation around Multi-Element Airfoils in Viscous Transonic Flow," ICAS Paper No. 80-11.3, 1980.

[12] Dougherty, F. C., Holst, T. L., Gundy, K. L., and Thomas, S. D., "TAIR—a Transonic Airfoil Analysis Computer Code," NASA TM-81296, 1981.

[13] Steger, J. L. and Baldwin, B. S., "Shock Waves and Drag in the Numerical Calculation of Isentropic Transonic Flows," NASA TN D-6997, 1972.

[14] Steger, J. L. and Sorenson, R. L., "Automatic Mesh-Point Clustering Near a Boundary in Grid Generation with Elliptic Partial Differential Equations, *Journal of Computational Physics*, Vol. 33, Dec. 1979, pp. 405-410.

[15] Sorenson, R. L., "A Computer Program to Generate Two-Dimensional Grids about Airfoils and Other Shapes by the Use of Poisson's Equation," NASA TM 81198, 1980.

[16] Flores, J., Holst, T. L., Kwak, D., and Batiste, D. M., "A New Consistent Spatial Differencing Scheme for the Transonic Full-Potential Equations," AIAA Paper 83-0373, 1983.

[17] South, J. C. Jr. and Hafez, M. M., "Stability Analysis of Intermediate Boundary Conditions in Approximate Factorization Schemes," AIAA Paper 83-1898-CP, 1983.

[18] Elfstrom, G. M., "Tests on a 15-in. Chord Cruise Augmentor Model (WTCC) in the NAE 15-in. × 60-in. Test Facility," Lab. Technical Report LTR-HA-5x5/0100, National Aeronautical Establishment (National Research Council Canada), Ottawa, Canada, March 1977, 1983.

[19] Farbridge, J., private communication, Dec. 1983.